Communications in Physics, Vol. 34, No. 4 (2024), pp. 317-332
DOI: https://doi.org/10.15625/0868-3166/21659

Effects of asymmetry in Kondo channels on thermoelectric efficiency

T. K. T. Nguyen[1,†], **T. B. Cao**[1], **T. A. Chu**[1], **T. L. H. Nguyen**[1], **H. Q. Nguyen**[1] **and M. N. Kiselev**[2]

[1]*Institute of Physics, Vietnam Academy of Science and Technology, 10 Dao Tan, Ba Dinh, Hanoi, Vietnam*

[2]*The Abdus Salam International Centre for Theoretical Physics, Strada Costiera 11, I-34151, Trieste, Italy*

E-mail: [†]nkthanh@iop.vast.vn

Received 4 October 2024

Accepted for publication 6 December 2024

Published 15 December 2024

Abstract. *We revisit an asymmetric two-channel charge Kondo model, which has been studied in the [Phys. Rev. B **82** (2010) 113306]. A nano-device modelling two-channel Kondo physics is a large metallic quantum dot which is embedded into a two-dimensional electron gas (2DEG) and connected strongly to two electrodes through two almost transparent single-mode quantum point contacts. The 2DEG is in the integer quantum Hall regime [Z. Iftikhar et al., Nature (London) **526** (2015) 233]. The reflection amplitudes at the quantum point contacts are asymmetric. We find that the thermopower and the figure of merit are decreased but the Kondo resonance width and Lorenz number in the vicinity of the Coulomb peak are lifted due to the effects of asymmetry in Kondo channels. We propose the method to improve the thermoelectric efficiency of the device.*

Keywords: thermoelectric transport; thermopower; thermal conductance; Lorenz number; figure of merit; charge Kondo effect.

Classification numbers: 73.23.Hk; 73.50.Lw; 72.15.Qm; 73.21.La.

1. Introduction

Thermoelectric materials generate electricity from temperature gradients, based on the Seebeck effect [1]. The mechanism of thermoelectric energy harvesting of the device is that when a temperature difference ΔT is applied, the charge carriers will diffuse from the hot side to the cold

side. As a result, an electrostatic potential ΔV_{th} is generated [2, 3]. However, the electrostatic potential generated by a bulk semiconductor, metal or alloy electronic component is very low (from a few milli-Volts to a few Volts). To achieve high voltage and power output, thermoelectric generators are often composed of dozens, even hundreds of pairs of thermoelectric components. The efficiency of thermoelectric materials is often measured by a dimensionless figure of merit ZT [4], which is defined as follows:

$$ZT = \frac{S^2 GT}{\mathscr{K}} \tag{1}$$

where $S = -\Delta V_{th}/\Delta T$ is the Seebeck coefficient or thermopower - a measure of the magnitude of an induced thermoelectric voltage in response to a temperature difference across the material, $G = \partial_V I_e|_{I_h=0}$ and $\mathscr{K} = \partial_{\Delta T} I_h|_{I_e=0}$ are the electrical conductance and thermal conductance, and T is the temperature of the system. In order to increase the thermoelectric efficiency, the system needs to be simultaneously enhanced thermopower and reduced thermal conductance. The investigation of thermal conductance goes beyond the study of thermopower. The relationship between thermal conductance and electric conductance is generalized in the Wiedemann-Franz (WL) law, characterized by the Lorenz number $L(T) \equiv \mathscr{K}/GT$. This implies that $ZT = S^2/L(T)$. For a macroscopic sample, $L_0 = \pi^2/3$. Transport through nanodevices is expected to violate the WF law even in the Fermi-liquid (FL) regime [5]. The Lorenz number in the quantum dot (QD) within the charge Kondo regime is reduced from a universal value at the particle-hole symmetric point, with the reduction being proportional to the square of thermopower [6].

The QDs are quantum systems where charge carriers are strongly confined in all three dimensions [7]. The first and most important transport phenomenon in QD devices is the Coulomb blockade effect, which occurs when the addition of an electron to the dot requires an energy greater than the charging energy $E_C = e^2/2C$, where C is the QD capacitance. At the Coulomb peaks, where the dimensionless gate voltage $N = CV_g/e$ (with V_g as the gate voltage) is a half-integer, the charge states of the QD are degenerate quadratically. These degenerate charge states can be considered as the two spin projections of a spin $S = 1/2$ quantum impurity, leading to the observation of a so-called charge Kondo effect [8–13]. For instance, in a system consisting of a large metallic QD strongly coupled to one (or several) lead(s) through an (or several) almost transparent single-mode quantum point contact(s) [QPC(s)], if the electron location is treated as an iso-spin variable, the backscattering at the quantum point contacts (QPCs) transfers the "moving in-" QD electrons to "moving out-" QD electrons and vice versa, resulting in an iso-spin flip. The number of different channels in the Kondo model is determined either by the spin projection quantum number of electrons [11] or by the number of single-mode QPCs [12, 13].

The Kondo channel number determines the properties of the Kondo system at temperatures below the Kondo temperature [14, 15]. Observables of the single-channel Kondo (1CK) system exhibit Fermi-liquid (FL) characteristics [16], while it is not the case for the observables of multi-channel Kondo (MCK) setups. These new non-Fermi liquid (NFL) behaviors attract the attention of physicists who are searching for and developing advanced thermoelectric materials.

It has been shown that the thermopower S in a charge Kondo circuit (CKC) is greatly enhanced compared to that of bulk metals [11, 17, 18]. The enhancement increases further when the Kondo channel number is raised from one to two [6, 11, 17] and the CKCs are scaled up to clusters [19–21]. In this paper, we examine the effects of asymmetry in Kondo channels on the thermopower S, Lorenz number $L(T)$, and the figure of merit ZT of an asymmetric two-channel

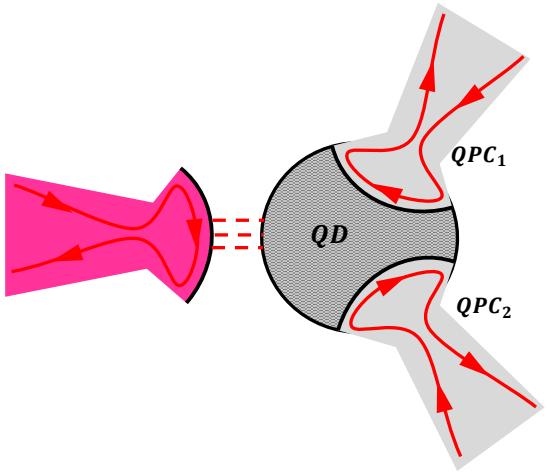

Fig. 1. Schematic of a charge Kondo circuit (CKC, grey color) is weakly coupled to a large electrode (pink color) through a tunnel barrier. The CKC consists of a large metallic island (QD, cross-hatched area), which is embedded in a two-dimensional electron gas (2DEG, plain area) and connects to two large electrodes through single-mode QPCs. These QPCs are controlled independently, so their reflection amplitudes generally differs from one another ($|r_1| \neq |r_2|$). The 2DEG is in the integer quantum Hall regime at the filling factor equals to 1 . The red line with arrows denotes the chiral edge mode, which backscatters at the center of the narrow constriction. The CKC is at a reference temperature T, while the left reservoir is at a higher temperature of $T + \Delta T$.

CKC (see Fig. 1). We find that the efficiency of a CKC is influenced by the reflection amplitudes at the QPCs but is only slightly affected by their difference.

The paper is organized as follows. We describe the theoretical model in Sec. II. Equations for the thermoelectric coefficients are presented and discussed in Sec. III. We conclude our work in Sec. IV.

2. General formulas for thermoelectric coefficients

In this section, we present the experimental implementation and general formulas for the thermoelectric coefficients. The corresponding theoretical model and detailed calculations for the thermoelectric coefficients have been demonstrated in Refs. [6, 11]. Therefore, we provide the final formulas for the reader's convenience.

2.1. Experimental setup and theoretical model

A two-channel charge Kondo device (see Fig. 1) was first theoretically proposed in Refs. [8, 9, 11] and later implemented in a breakthrough experiment [12]. The QD, formed by a large metallic island (the cross-hatched area surrounded by the black line), is electronically connected to a 2DEG (the pink and gray continuous areas). The 2DEG is connected to two large electrodes through two QPCs. Applying a strong magnetic field perpendicular to the 2DEG plane can control the 2DEG in the integer quantum Hall regime at the filling factor equals to 1. The QPCs are

fine-tuned (by field effects in the split gates, not shown here) to the high transparency regime corresponding to weak backscattering ($|r_j| \ll 1$, $j = 1,2$) of the chiral edge mode (red solid lines with arrows). In general, $|r_1| \neq |r_2|$ indicates that the CKC is in the asymmectric two-channel regime. The symmetric case occurs when $|r_1| = |r_2| = |r|$. The CKC at the reference temperature T, is weakly coupled to a large electrode that is at a higher temperature of $T + \Delta T$ (pink color) through a tunnel barrier. The temperature drops at the weak link.

Hamiltonian describing the two-channel charge Kondo device (see Fig. 1) in which the QD coupled weakly to the left lead and strongly to the two other ones on the right side through two QPCs, has form

$$H = H_0 + H_C + H_L + H_R \tag{2}$$

where H_0 characterizes electrons in QD and in the left (L) and two right (R) leads,

$$H_0 = \sum_k \varepsilon_k a_k^\dagger a_k + \sum_p \varepsilon_p d_p^\dagger d_p + i v_F \sum_{\alpha,\lambda} \int_{-\infty}^{\infty} dx \psi_{\alpha,\lambda}^\dagger \partial_x \psi_{\alpha,\lambda}. \tag{3}$$

Here, a_k and d_p denote the spinless electrons in the left lead and in the QD at the left tunnel barrier, correspondingly. The third term in Eq. (3) describes the one-dimensional electrons in the two right contacts (two QPCs named in Fig. 1) (in $\hbar = k_B = e = 1$ units). $\psi_{\alpha,\lambda}$ are operators describing one-dimensional fermions in the QPCα (with $\alpha = 1,2$), the iso-spin index λ takes values $\lambda = \uparrow$ for electrons in the QD-QPC and $\lambda = \downarrow$ for electrons in the right electrodes, v_F is Fermi velocity.

Second term in the Eq. (2), the so-called charging Hamiltonian, describes the Coulomb interaction in the QD,

$$H_C = E_C \left[\hat{n}_L + \hat{n}_R - N\right]^2, \tag{4}$$

where $E_C = e^2/2C$ is the charging energy (C is the QD capacitance), $\hat{n}_L$ is the integer-value operator of electrons entered through the left (tunnel) contact, while $\hat{n}_R = \sum_\alpha \psi_{\alpha,\uparrow}^\dagger \psi_{\alpha,\uparrow}$ denotes the number operator ofthe electrons entered through the two QPCs (from the two right leads), N is dimensionless parameter controlled by the gate voltage V_g as $N = CV_g/e$.

The tunnel Hamiltonian, which describes the weak coupling between the left lead and the QD, reads

$$H_L = \sum_{k,p} (t_{LD} a_k^\dagger d_p \hat{F} + h.c.), \tag{5}$$

where $t_{LD} \ll 1$ is hopping amplitude and $\hat{F}$ is the charge-lowering operator, which obeys the commutation relation $\left[\hat{F}, \hat{n}_L\right] = \hat{F}$. We notice that the operator d_p can be expressed through the fermionic operator in the 1D system as $\sum_p d_p^\dagger d_p \to \sum_\alpha \psi_{\alpha,\uparrow}^\dagger(-\infty)\psi_{\alpha,\uparrow}(-\infty)$ with $\psi_{\alpha,\uparrow}(x) \sim e^{i\phi_\alpha(x)}$.

The Hamiltonian H_R demonstrating the backward scattering in the QPCs on the right side is written as

$$H_R = \sum_\alpha \int_\infty^\infty dx \left[\psi_{\alpha,\uparrow}^\dagger(x) V_\alpha(x) \psi_{\alpha,\downarrow} e^{-i2k_F x} + \text{h.c.}\right], \tag{6}$$

where $V_\alpha(x)$ is a short range QPCα' isospin-flip potential. The reflection amplitudes of the QPCα is determined by $|r_\alpha| = V_\alpha(2k_F)/v_F$ (k_F is Fermi momentum).

2.2. *The formulas*

To study the thermoelectric effects at the weak link between the left electrode and the QD in the linear response regime $[\Delta T, e\Delta V_{th}] \ll T$, we consider both the charge current I_e and the heat current I_h across the tunnel contact:

$$\begin{pmatrix} I_e \\ I_h \end{pmatrix} = \begin{pmatrix} L_{ee} & L_{eh} \\ L_{he} & L_{hh} \end{pmatrix} \begin{pmatrix} \Delta V \\ \Delta T \end{pmatrix}, \tag{7}$$

where L_{ij} are thermoelectric coefficients which are related to the Onsager factors [22] . In fact, L_{ee} is the electric conductance, L_{eh} is the thermoelectric coefficient, so thermopower S and thermal conductance $\mathscr{K}$ are written as follows

$$S = \frac{L_{eh}}{L_{ee}}, \quad \mathscr{K} = L_{hh} - T\frac{L_{eh}^2}{L_{ee}}. \tag{8}$$

The Lorenz number is written as

$$L(T) = \frac{L_{hh}}{TL_{ee}} - S^2. \tag{9}$$

To gain a better understanding of thermal conductance and figure of merit, we define the Mahan-Sofo (MS) factor as [23]

$$ms = T\frac{L_{eh}^2}{L_{hh}L_{ee}} = \frac{TL_{ee}}{L_{hh}}S^2. \tag{10}$$

The Lorenz number and the figure of merit in the linear regime are expressed as functions of ms as

$$L(T) = \frac{L_{hh}}{TL_{ee}}(1 - ms), \tag{11}$$

$$ZT = \frac{ms}{1 - ms}. \tag{12}$$

The MS factor must be dimenssionless and satisfies $0 < ms < 1$. It is straightforward to see that the figure of merit ZT reaches its maximum value when the MS factor approaches 1.

The computations for the above currents involve the local density of states (DoS) $\nu(\epsilon)$ of the QD at the weak link. The currents are considered in the linear response regime and are computed based on the DoS, the Fermi distribution functions of the QDs at the weak link, and the tunnel matrix element $|t_{LD}|$, which characterizes the weak coupling between the left electrode and the QD. In the spirit of Matveev-Andreev theory [11], the DoS $\nu(\epsilon)$ is related to the correlation function $K(1/2T + it)$, which describes the interactions in the QD

$$\nu(\epsilon) = \nu_D T \cosh\left(\frac{\epsilon}{2T}\right)\int_{-\infty}^{\infty} \frac{e^{i\epsilon t}K\left(\frac{1}{2T} + it\right)}{\cosh(\pi T t)}dt, \tag{13}$$

where ν_D stands for the DoS of the QD which is no longer renormalized by the electron-electron interactions, while the correlation function $K(1/2T + it)$ characterizes for these interactions [$K(\tau) = \langle T_\tau \hat{F}(\tau)\hat{F}^\dagger(0)\rangle$ (T_τ is the time-ordering operator, the imaginary time τ runs from 0 to $\beta = 1/T$)]. The details of the derivatation for the electric conductance and thermoelectric coefficient are presented in Refs. [6, 11]. Finally, one can express the formulas for the thermoelectric coefficients

as

$$L_{ee} = \frac{\pi}{2} G_L T \int_{-\infty}^{\infty} dt \frac{K\left(\frac{1}{2T} + it\right)}{\cosh^2(\pi T t)}, \tag{14}$$

$$L_{eh} = -\frac{i\pi^2 G_L T}{2} \int_{-\infty}^{\infty} dt \frac{\sinh(\pi T t)}{\cosh^3(\pi T t)} K\left(\frac{1}{2T} + it\right), \tag{15}$$

$$L_{hh} = \frac{\pi^3 G_L T^2}{2} \int_{-\infty}^{\infty} dt \frac{\left[2 - \cosh^2(\pi T t)\right] K\left(\frac{1}{2T} + it\right)}{\cosh^4(\pi T t)}. \tag{16}$$

where $G_L = 2\pi \nu_L \nu_D |t_{LD}|^2$ (ν_L stands for the DoS of the non-interacting left lead) is a conductance of the tunnel area, assuming that the electrons in the left lead and QD are noninteracting.

The computation of the thermoelectric coefficients in Eqs. (14-16) requires the explicit form of the correlation functions $K(1/2T + it)$. These correlation functions were first computed using the perturbation theory, considering the smallness of the reflection amplitudes $|r_j|$ of the QPCs in the temperature regime: $\max\left[|r_j|^2 E_C\right] \ll T \ll E_C$. The thermoelectric transport of a 2CK system is controlled by (bosonic) charge and spin fluctuations at low frequencies (below E_C). We notice that the effect of small $|r_j|$ on the charge modes is negnigible in comparison with the Coulomb blockade; however, it dramatically alters the dynamics of the unblocked spin modes. Therefore, it is neccessary to investigate the spin modes by applying the refermionization method. The procedure beyond the perturbative solution is referred to as nonperturbative treatment [11]. Previous works (see Refs. [11, 17, 21]) have shown that the results of the nonperturbative solution recover the perturbative results. It is thus sufficient to consider the problem in a nonperturbative treatment.

3. Main results

In this section, we present the obtained formulas for the Onsager coefficients and the MS factor using the nonperturbative method. It is important to estimate the input parameters and select the appropriate value for the figure of merit ZT.

The correlation function for the two-channel CKC in the nonperturbative treatment, concerning the reflection amplitudes of the QPCs, is expressed as [11]

$$\begin{aligned} K(\tau) = {} & \frac{\pi T \Gamma}{\gamma E_C} \frac{1}{|\sin(\pi T \tau)|} \int_{-\infty}^{\infty} \frac{e^{\omega\tau}}{(\omega^2 + \Gamma^2)\left(1 + e^{\omega/T}\right)} d\omega \\ & - \frac{T}{E_C}\left(s^2 - a^2\right) \frac{\sin(2\pi N)}{|\sin(\pi T \tau)|} \ln\left(\frac{E_C}{T + \Gamma}\right) \int_{-\infty}^{\infty} d\omega \frac{\omega e^{\omega\tau}}{(\omega^2 + \Gamma^2)\left(1 + e^{\omega/T}\right)}, \end{aligned} \tag{17}$$

with $s = |r_1| + |r_2|$, $a = ||r_1| - |r_2||$, Γ is the Kondo-resonance width in the vicinity of Coulomb peaks

$$\Gamma(N) = \frac{2\gamma E_C}{\pi^2}\left[s^2 \cos^2(\pi N) + a^2 \sin^2(\pi N)\right], \tag{18}$$

and $\gamma = e^{\mathbf{C}} \approx 1.78$ ($\mathbf{C} \approx 0.577$ is Euler's constant). Following Ref. [17], the Kondo resonance width at a Coulomb peak is always finite for any asymmetry in the Kondo channels.

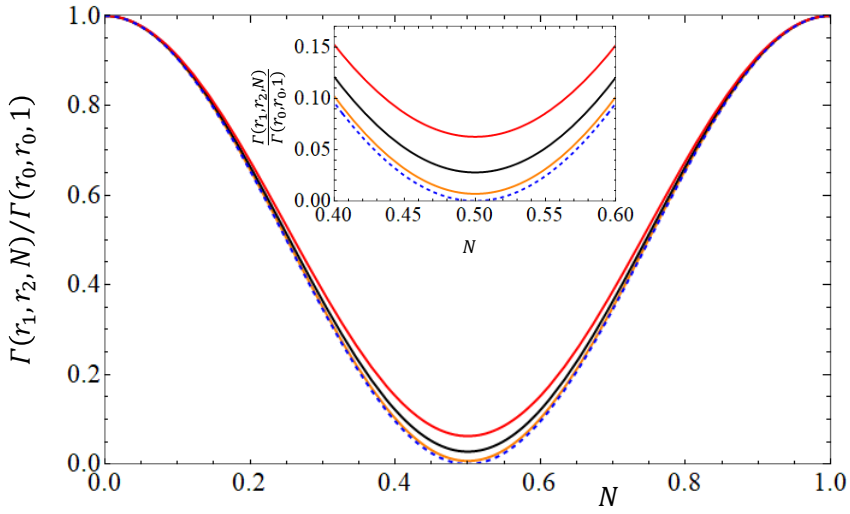

Fig. 2. The Kondo-resonance width $\Gamma(r_1, r_2, N)/\Gamma(r_0, r_0, 1)$ as a function of gate voltage N for different asymmetric reflection amplitude set $r_1 = 0.13, r_2 = 0.11$ (orange line), $r_1 = 0.14, r_2 = 0.1$ (black line), $r_1 = 0.15, r_2 = 0.09$ (red line), and reference symmetric set $r_0 = 0.12$ (blue dashed line). The insert is the zoomed in of the main plots in the vicinity of the Coulomb peak.

We find that the first term of the correlation function $K(\tau)$ is symmetric in energy, while the second one is asymmetric. It is sufficient to consider the first term in Eq. (17) to compute L_{ee} and L_{hh}, but the second term in Eq. (17) must be taken into account for the L_{eh} calculation. The thermoelectric coefficients are obtained as

$$L_{ee} = \frac{G_L T}{8\gamma E_C} F_G\left(\frac{\Gamma}{T}\right), \tag{19}$$

with F_G is a dimensionless function expressed as

$$F_G(p) = \int_{-\infty}^{\infty} du \frac{p}{u^2 + p^2} \frac{u^2 + \pi^2}{\cosh^2(u/2)}, \tag{20}$$

where $p = \Gamma/T$, $u = \omega/T$. The L_{eh} is computed as

$$L_{eh} = -\frac{G_L}{24\pi} \frac{T}{E_C} \left(s^2 - a^2\right) \sin(2\pi N) \ln\left(\frac{E_C}{T + \Gamma}\right) F_T\left(\frac{\Gamma}{T}\right), \tag{21}$$

with

$$F_T(p) = \int_{-\infty}^{\infty} du \frac{u^2}{u^2 + p^2} \frac{u^2 + \pi^2}{\cosh^2(u/2)}. \tag{22}$$

The L_{hh} can be expressed as

$$L_{hh} = \frac{G_L}{48\gamma} \frac{T^2}{E_C} F_H\left(\frac{\Gamma}{T}\right), \tag{23}$$

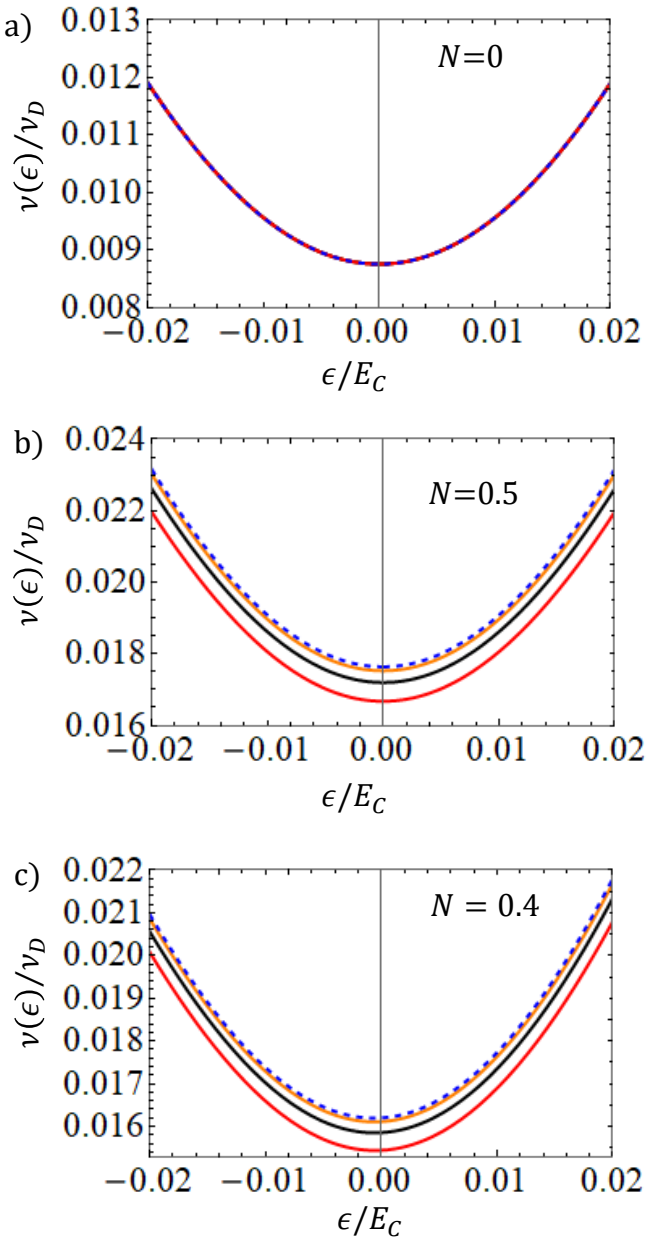

Fig. 3. Density of states $\nu(\epsilon)/\nu_D$ as a function of energy ϵ/E_C for different values of the gate voltage: $N = 0$ or $N = 1$ [panel a)], $N = 0.5$ [panel b)], and $N = 0.4$ [panel c)]. All plots are at temperature $T/E_C = 0.01$, for different asymmetric reflection amplitude set $r_1 = 0.13, r_2 = 0.11$ (orange line), $r_1 = 0.14, r_2 = 0.1$ (black line), $r_1 = 0.15, r_2 = 0.09$ (red line), and reference symmetric set $r_0 = 0.12$ (blue dashed line).

with

$$F_H(p) = \int_{-\infty}^{\infty} du \frac{p}{u^2+p^2} \frac{\left(u^2+\pi^2\right)\left(u^2+3\pi^2\right)}{\cosh^2(u/2)}. \tag{24}$$

The MS factor is obtained as

$$ms = \frac{2\gamma^2}{3\pi^2}\left(s^2-a^2\right)^2 \sin^2(2\pi N) \ln^2\left(\frac{E_C}{T+\Gamma}\right) \frac{F_T^2\left(\frac{\Gamma}{T}\right)}{F_H\left(\frac{\Gamma}{T}\right) F_G\left(\frac{\Gamma}{T}\right)}. \tag{25}$$

From Eq. (25), we find that $0 < ms < 0.3337|r_1|^2|r_2|^2 \ln^2[E_C/(T+\Gamma)]$, so the MS factor is predicted much smaller than 1. Therefore, we estimate $ZT_{max} \approx 0.33|r_1|^2|r_2|^2 \ln^2[E_C/2\Gamma]$ at the temperature $T \approx \Gamma$. It is consistent with the result in Ref. [21].

The motivation of this work is to investigate the effects of asymmetry in the Kondo channels on quantum transport in the CKC. We thus choose the reference reflection amplitude $r_0 = (r_1 + r_2)/2$ as the symmetric case for the corresponding asymmetric r_1, r_2. We first examine this for the Kondo resonance width (see Fig. 2). In the vicinity of the Coulomb peaks, the asymmetry in the Kondo channels lifts the Kondo resonance width [17]. The greater the asymmetry, the higher the value of Γ. This fact can be seen easily when one rewrites Eq. (18) as $\Gamma(N) = (2\gamma E_C/\pi^2)[|r_1|^2 + |r_2|^2 + 2|r_1||r_2|\cos(2\pi N)]$. At the Coulomb peak $N = 0.5$, we have $\Gamma(0.5) = (|r_1| - |r_2|)^2 \geq 0$. The finite gap at $N = 0.5$ characterizes for the spin mode. It means that both charge and spin modes in the asymmetric two channel Kondo model are massive. The finite channel asymmetry results in a crossover from the non-Fermi liquid (NFL) behavior (symmetric case) to Fermi liquid (FL) behavior (asymmetric case) (this effect is discussed in detail in Ref. [17]). The crossover is triggered by the appearance of a finite Majorana level width at the Coulomb peak position [$\propto \sin^2(\pi N)$]. The value of the gap corresponds to the energy scale below which the FL properties of the model are restored. The NFL-2CK intermediate coupling fixed point is hyperbolic (unstable). The channel asymmetry is a relevant perturbation that drives the system away from the unstable 2CK fixed point to the stable FL-1CK strong coupling fixed point.

In order to check more the effects channel asymmetry to thermoelectric transport, we plot the DoS as a function of energy in Fig. 3. In panels a) and b), where the DoS is plotted at the Coulomb valley ($N = 0$ or $N = 1$) and Coulomb peak ($N = 0.5$), one can observe symmetry in energy. This explains why the thermopower vanishes at these points. In the vicinity of the Coulomb peak, an asymmetry in energy appears, as shown in panel c). We also find that when the asymmetry between the two Kondo channels (characterized by a/r_0) increases, the DoS decreases. Furthermore, we predict that the asymmetry between the two Kondo channels does not affect the symmetry in energy of the DoS.

Applying this fact to Eqs. (20), (22) and (24) at a given temperature, we consider the ratios F_T/F_G, F_H/F_G, and $F_T^2/F_H F_G$ as functions of $p = \Gamma/T$, which are demonstrated in Fig. 4. We predict that the asymmetry in the Kondo channels reduces the thermopower, MS factor, and figure of merit, but increases the Lorenz number.

Figure 5 shows the thermopower S as a function of gate voltage N (upper panel) and the maximum of thermopower S_{max} as a function of temperature T/E_C (lower panel) for different sets of asymmetric reflection amplitude compared to the reference symmetry set. When the asymmetry is increased, especially when a/r_0 is large enough, the thermopower is visibly decreases.

The results we obtained for the Lorenz number (see Fig. 6) align with those discussed in Ref. [6]: the Lorenz number is reduced from a universal value corresponding to the particle-hole

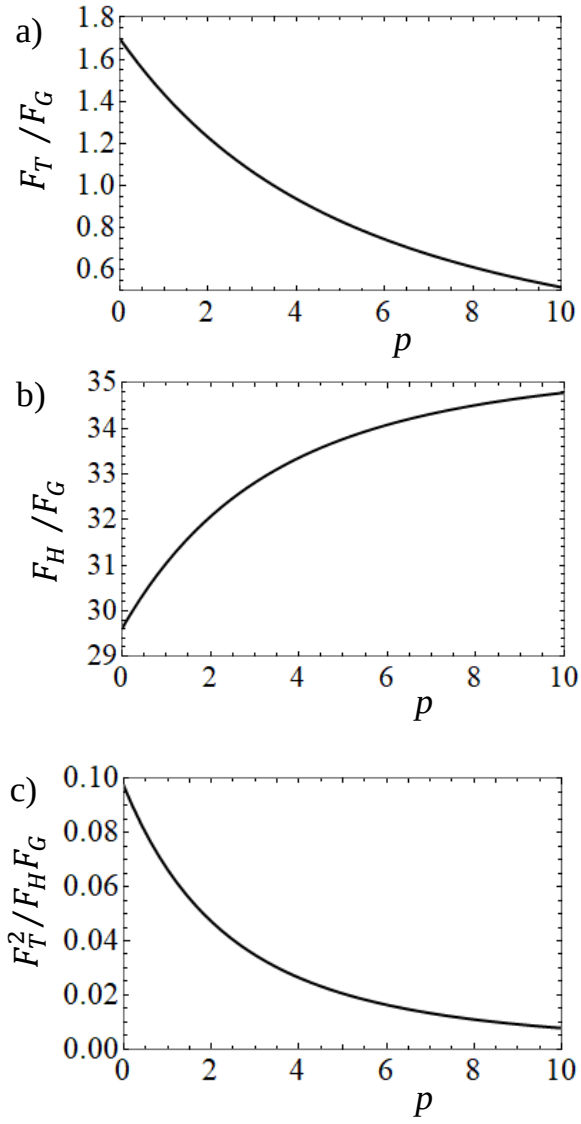

Fig. 4. The ratios F_T/F_G [panel a)], F_H/F_G [panel b)], and F_T^2/F_HF_G [panel c)] as functions of variable $p = \Gamma/T$.

symmetric point. The decrease in the Lorenz number with increasing temperature depends on the temperature region: it is significant at low temperatures and less pronounced at higher temperatures (see Fig. 6 b) as an example). Moreover, we also show in Fig. 6 a) that the Lorenz number in the vicinity of the Coulomb peak is increased slightly by a/r_0. The Lorenz ratio $L(T)/L_0$, which is always equal to or greater than 1.5 as it is shown in Fig. 6 c), satisfies the generalized WF law at

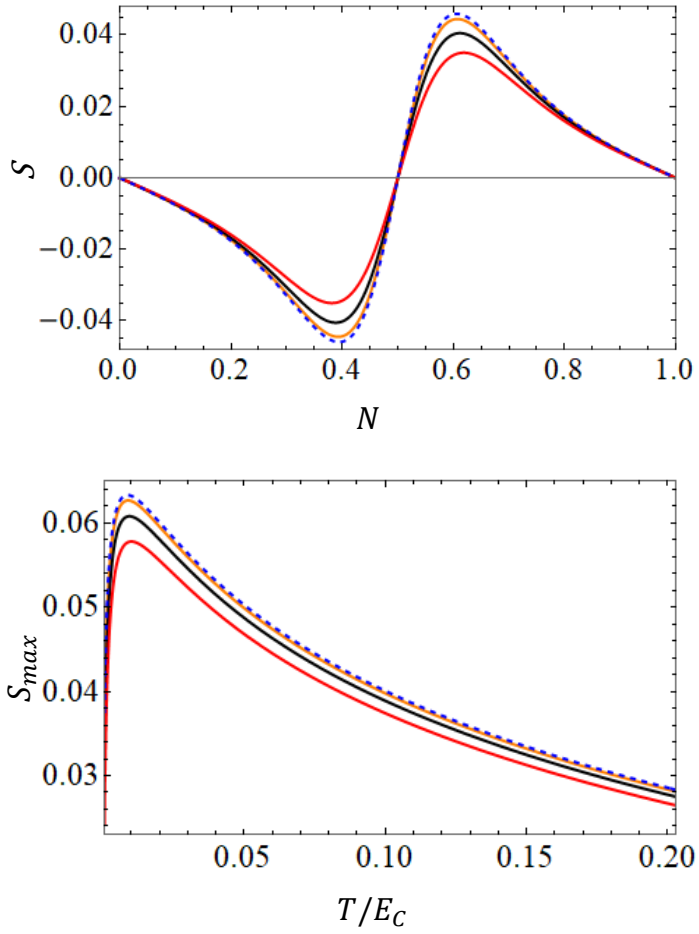

Fig. 5. The thermopower S as a function of gate voltage N at temperature $T/E_C = 0.01$ (upper panel) and maximum of thermopower S_{max} as a function of temperature T/E_C (lower panel) for different asymmetric reflection amplitude set $r_1 = 0.13, r_2 = 0.11$ (red line), $r_1 = 0.14, r_2 = 0.1$ (black line), $r_1 = 0.15, r_2 = 0.09$ (orange line), and reference symmetric set $r_0 = 0.12$ (blue dashed line).

low temperature in the case of strong electron-electron correlations. This confirms the conclusion in Ref. [24] that Lorenz ratios contain information of the Anderson's orthogonality catastrophe.

We plot the figure of merit ZT as a function of the gate voltage N [Figs. 7 a) and b), and 8 a)] and its maximum as a function of temperature T/E_C [Figs. 7 c) and 8 b)]. The parameters in Fig. 7 indicate that ZT reaches maximum values at the gate voltage N situated between Coulomb peak and Coulomb valley (covering the perturbative solution). They approach the Coulomb peak as the temperature is reduced to zero, where only the nonperturbative treatment is applicable. From

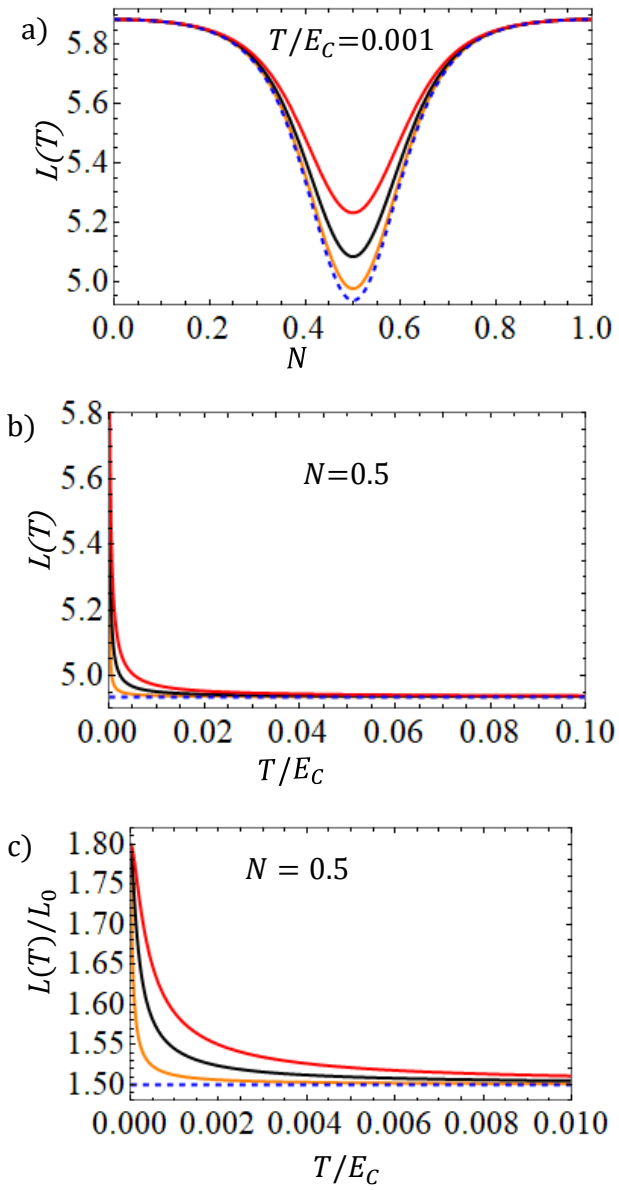

Fig. 6. a) Lorenz number $L(T)$ as a function of gate voltage N at temperature $T/E_C = 0.001$. b) $L(T)$ as a function of temperature T/E_C at gate voltage $N = 0.5$. c) Ratio $L(T)/L_0$ as a function of temperature T/E_C at gate voltage $N = 0.5$. All plots are for different asymmetric reflection amplitude set $r_1 = 0.13, r_2 = 0.11$ (orange line), $r_1 = 0.14, r_2 = 0.1$ (black line), $r_1 = 0.15, r_2 = 0.09$ (red line), and reference symmetric set $r_0 = 0.12$ (blue dashed line).

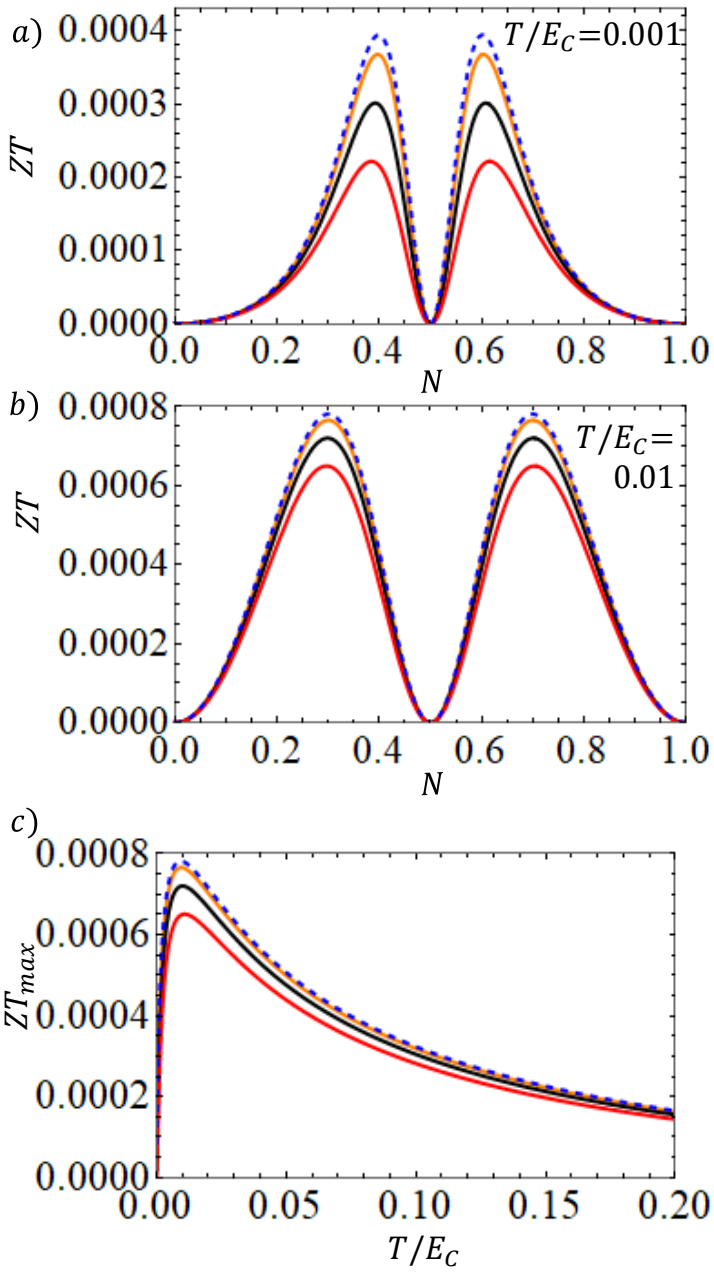

Fig. 7. Figure of merit ZT as a function of gate voltage N at different temperatures: $T/E_C = 0.001$ [panel a)], $T/E_C = 0.01$ [panel b)], and maximum of figure of merit ZT_{max} as a function of temperature T/E_C [panel c)], for different asymmetric reflection amplitude set $r_1 = 0.13, r_2 = 0.11$ (orange line), $r_1 = 0.14, r_2 = 0.1$ (black line), $r_1 = 0.15, r_2 = 0.09$ (red line), and reference symmetric set $r_0 = 0.12$ (blue dashed line).

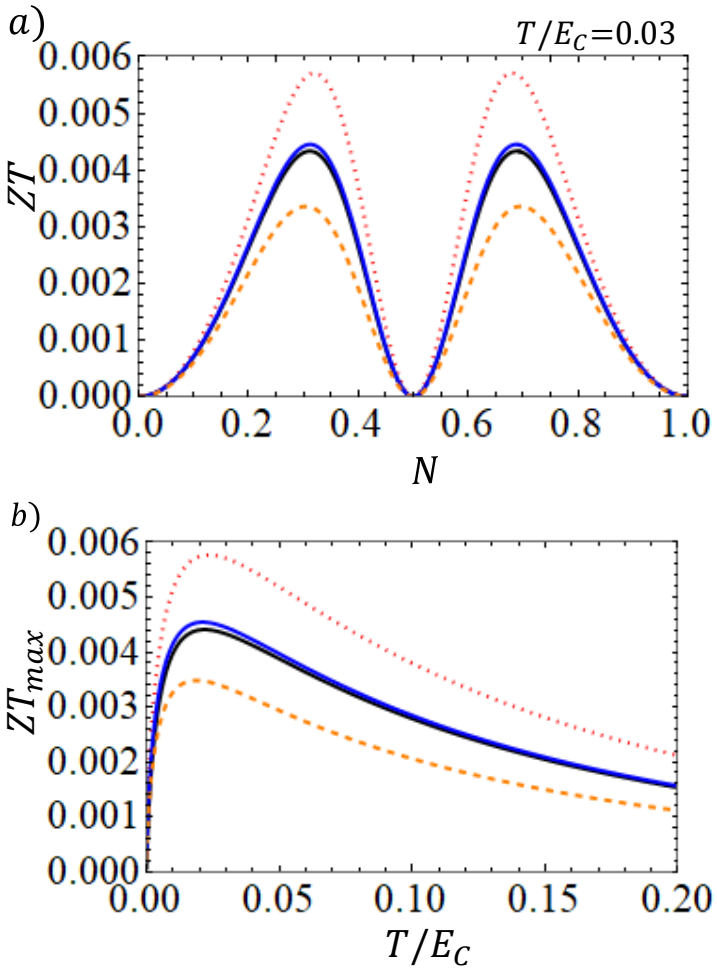

Fig. 8. Figure of merit ZT as a function of gate voltage N at temperature $T/E_C = 0.03$ [panel a)], and maximum of figure of merit ZT_{max} as a function of temperature T/E_C [panel c)], for different reflection amplitude set $r_1 = r_2 = 0.24$ (red dotted line), $r_1 = r_2 = 0.22$ (blue line), $r_1 = 0.24, r_2 = 0.2$ (black line), and $r_1 = r_2 = 0.2$ (orange dashed line).

Figs. 7 c) and 8 b), we predicts that the maximum figure of merit ZT_{max} attains its highest value at $T/E_C \approx 0.03$. We find that ZT and ZT_{max} decrease as the asymmetry a/r_0 increases compared to their values at r_0 (see Fig. 7). Additionally, Fig. 8 shows that ZT and ZT_{max} increase when the average of the reflection amplitudes $|r_0|$ is raised. However, the constraints of the model require that $|r_j|$ be small enough. Therefore, we conclude that the figure of merit of a single-site CKC is much smaller than 1.

As we can see from Fig. 7 c), the temperature regime $|r_0|^2 E_C \ll T \ll E_C$, along with the smallness of the reflection amplitude $|r_0|$, satisfies the condition for applying the perturbative solution, but is not the optimal range for maximizing the figure of merit ZT. This suggests that

we should consider the thermoelectric efficiency of the charge Kondo circuits in the vicinity of the intermediate coupling fixed point which requires non-perturbative analysis.

4. Conclusion

In summary, we revisited the thermoelectric transport of a system in which a single-site CKC is weakly coupled to a large electrode through a tunnel barrier. The temperature drops at the weak link [6, 11, 17]. The CKC consists of a large QD strongly coupled to the electrodes through two QPCs [12]. The reflection amplitudes at the QPCs are asymmetric ($|r_1| \neq |r_2|$) [17]. In the spirit of Andreev-Matveev theory [11], we apply the Abelian bosonization and refermionization technique to solve the 2CK model nonperturbatively. We present the formulas for the thermoelectric coefficients and the MS factor. The thermopower, figure of merit, and their maximum values are illustrated in graphics. The Lorenz number is also investigated. We conclude that the thermopower, MS factor, and figure of merit are reduced, while the Lorenz number is increased slightly due to the asymmetry in the Kondo channels. It is important to tune the reflectrion amplitudes at the QPCs to be symmetric. Furthermore, we propose scaling up the CKCs to clusters or lattices to enhance the thermoelectric efficiency of an implemented device.

Acknowledgements

This research in Hanoi is funded by Vietnam Academy of Science and Technology (program for Physics development) under grant number KHCBVL.06/23-24.

References

[1] T. J. Seebeck, *Über den Magnetismus der galvanischen Kette*, Abh. Akad. Wiss. Berlin **1820-21** (1822) 289.
[2] J. F. Li, W.S. Liu, L.D. Zhao, M. Zhou, *High-performance nanostructured thermoelectric materials*, NPG Asia Mater. **2** (2010) 152.
[3] Y. Du, K. F. Cai, S. Chen, H. Wang, S. Z. Shen, R. Donelson, T. Lin, *Thermoelectric fabrics: toward power generating clothing*, Sci. Rep. **5** (2015) 6144.
[4] A. J. Minnich, M. S. Dresselhaus, Z. F. Ren, G. Chen, *Bulk nanostructured thermoelectric materials: current research and future prospects*, Energy Environ. Sci. **2** (2009) 466.
[5] G. Benenti, G. Casati, K. Saito, and R. Whitney, *Fundamental aspects of steady-state conversion of heat to work at the nanoscale*, Phys. Rep. **694** (2017) 1.
[6] D. B. Karki, *Coulomb blockade oscillations of heat conductance in the charge Kondo regime*, Phys. Rev. B**102** (2020) 245430.
[7] *Single Charge Tunneling: Coulomb Blockade Phenomena in Nanostructures*, H. Grabert and M. H. Devoret, Plenum Press, New York (1992).
[8] K. Flensberg, *Capacitance and conductance of mesoscopic systems connected by quantum point contacts*, Phys. Rev. B **48** (1993) 11156.
[9] K. A. Matveev, *Coulomb blockade at almost perfect transmission*, Phys. Rev. B **51** (1995) 1743.
[10] A. Furusaki, K. A. Matveev, *Theory of strong inelastic cotunneling*, Phys. Rev. B **52** (1995) 16676.
[11] A. V. Andreev, K. A. Matveev, *Coulomb blockade oscillations in the thermopower of open quantum dots*, Phys. Rev. Lett. **86** (2001) 280; *Thermopower of a single-electron transistor in the regime of strong inelastic cotunneling*, Phys. Rev. B **66** (2002) 045301.
[12] Z. Iftikhar, S. Jezouin, A. Anthore, U. Gennser, F. D. Parmentier, A. Cavanna and F. Pierre, *Two-channel Kondo effect and renormalization flow with macroscopic quantum charge states*, Nature **526** (2015) 233.
[13] Z. Iftikhar, A. Anthore, A. K. Mitchell, F. D. Parmentier, U. Gennser, A. Ouerghi, A. Cavanna, C. Mora, P. Simon, and F. Pierre, *Tunable quantum criticality and super-ballistic transport in a "charge" Kondo circuit*, Science **360** (2018) 1315.

[14] A. Hewson, *The Kondo Problem to Heavy Fermions, Cambridge Studies in Magnetism*, Cambridge University Press, Cambridge, 1993.
[15] P. Nozières and A. Blandin, *Kondo effect in real metals*, J. Phys. France **41** (1980) 193.
[16] L. D. Landau, *The Theory of a Fermi Liquid*, Sov. Phys. JETP **3** (1957) 920.
[17] T. K. T. Nguyen, M. N. Kiselev, and V. E. Kravtsov, *Thermoelectric transport through a quantum dot: Effects of asymmetry in Kondo channels*, Phys. Rev. B **82** (2010) 113306.
[18] R. Scheibner, H. Buhmann, D. Reuter, M. N. Kiselev, and L. W. Molenkamp, *Thermopower of a Kondo spin-correlated quantum dot*, Phys. Rev. Lett. 95 (2005) 176602.
[19] T. K. T. Nguyen and M. N. Kiselev, *Seebeck effect on a weak link between Fermi and non-Fermi liquids*, Phys. Rev. B **97** (2018) 085403.
[20] T. K. T. Nguyen and M. N. Kiselev, *Heat conductance oscillations in two weakly connected charge Kondo circuits*, Comm. Phys. **32**, 331 (2022).
[21] T. K. T. Nguyen, H. Q. Nguyen, and M. N. Kiselev, *Thermoelectric transport across a tunnel contact between two charge Kondo circuits: Beyond perturbation theory*, Phys. Rev. B **109** (2024) 115139.
[22] L. Onsager, *Reciprocal relations in irreversible processes. I.*, Phys. Rev. **37**, 405 (1931); L. Onsager, *Reciprocal relations in irreversible processes. II.*, Phys. Rev. **38** (1931) 2265.
[23] G. D. Mahan and J. O. Sofo, *The best thermoelectric*, Proc. Natl. Acad. Sci. USA **93** (1996) 7436.
[24] M. N. Kiselev, *Generalized Wiedemann-Franz law in a two-site charge Kondo circuit: Lorenz ratio as a manifestation of the orthogonality catastrophe*, Phys. Rev. B **108** (2023) L081108.